Dry and Grease-Lubricated Reciprocating Wear Resistance of Laser-

Clad FeCrMoCB Amorphous Coating on AISI 52100 Steel

1.0 Introduction

1

2

3

4 5

6

7

8

9

10

11

12

13

14

15

16

17

18

19

20

21

22

23

24

25

26

27

The demand for wear-resistant materials is rising rapidly in high-performance sectors like automotive, aerospace, and industrial machinery. AISI 52100 steel is a high-hardness and fatigue-resistant steel that has been widely used in the manufacturing of bearings and rolling elements. Despite its interesting properties, AISI 52100 steel is vulnerable to severe wear and surface damage in high friction and sliding contact environments. Therefore, improving the wear resistance of AISI 52100 steel is essential in order to enhance the reliability and service life of machine components exposed to tribological loads [1]. This challenge is a common opportunity for advanced surface engineering techniques, including laser cladding. Laser cladding is a versatile surface engineering technique enabling protective coatings to be deposited on various metallic substrates [2]. It offers advantages such as strong metallurgical bonding, minimal dilution, and precise control over coating thickness and microstructure. Studies have shown that Fe-based amorphous coatings generally outperform crystalline coatings in high-wear applications, particularly in harsh conditions where AISI 52100 steel is used [3], [4]. While advanced hard coatings such as WC-Co, CrN, and Ni-based alloys have been widely applied to improve the wear performance of steels, they are prone to cracking and delamination due to physical properties mismatch with the substrate. FeCrMoCB amorphous coatings has promising tribological properties, in addition they exhibit similar composition reducing the possibilities of cracking and delamination. Moreover, FeCrMoCB coatings on bearing-grade AISI 52100 steel remains largely unexplored. This study specifically addresses this gap by investigating the unique tribological response of this novel coating-substrate system under dry and grease-lubricated reciprocating conditions. The previous studies have reported promising results for Fe-based amorphous coatings applied via laser cladding, research on their wear performance under different lubrication conditions particularly dry compared to grease-

lubricated, is still limited. Previous studies have been mainly limited to wear resistance in only one lubrication

condition without comparative analysis, which hinders the understanding of underlying wear mechanisms and coating

durability under different lubrication conditions [2], [5]. Since lubrication plays a vital role in wear control and

improving component life, it is important to investigate the influence of different lubrication conditions on Fe-based

amorphous coatings. It is particularly important in reciprocating wear cases, i.e., where materials come to repetitive sliding or cyclic contact with one another, as in engines, pumps, and several types of industrial machinery [6], [7]. This study distinguishes itself by integrating laser-clad FeCrMoCB amorphous coatings on fatigue-prone AISI 52100 steel and evaluating their tribological performance under industrial relevant reciprocating wear regimes. Unlike previous studies focused on single-condition tests, the studies systematically contrasts dry and grease-lubricated behavior, revealing grease-induced reductions in wear volume exceeding 40%, a finding not reported in prior literature [8]. This study provides new insights into the tribological behavior of Fe-based amorphous coatings, contributing to the development of more durable and efficient coating systems for industrial applications requiring superior wear resistance and reliability under varied operating conditions. [9], [10].

2.0 Materials and Methods

2.1 Materials

AISI 52100 steel with dimensions $15 \times 15 \times 4$ mm for each of the nine sample coatings was used in this research as a substrate material characterized by high carbon and chromium content, leading to its high hardness and fatigue resistance. Optical emission spectrometry analysis of the steel show a composition of carbon 1.0% carbon and 1.5% chromium, with traces of other elements [11]. The Fe-based coating, composed of linear-grooved iron (Fe), chromium (Cr) and molybdenum (Mo), with trace amounts of carbon (C) and boron (B), was prepared using the powder metallurgy method [12]. The coating material was a FeCrMoCB amorphous powder from LiquidMetal Coatings® with a nominal particle size of 20– $80 \mu m$. For this purpose, the powder composition (composed of Fe, Cr, Mo, C and B) was optimized to provide high amorphous content in the final layer of cladding, which greatly increases hardness and wear resistance [13], [14], [15].

2.2 Laser cladding process

The AISI 52100 steel substrates were polished to a mirror-like surface with silicon carbide papers, ranging from 400 to 1200 grit, prior to the application of the coating. The substrates were then cleaned in an ultrasonic bath containing acetone to remove any surface contaminants, followed by drying with compressed air [16]. The samples were manufactured in a fiber laser system (ROFIN StarFiber 300, Germany), working at a maximum power of 300 W and a wavelength of 1070 ± 10 nm. Figure 1(a), (b), and (c) shows the laser cladding (LC) setup with pre-applied powder, laser scanning direction and overlap areas, and images of samples before and after cladding, respectively. A 15 L/min

argon flow [17] was used as a protective gas, with a fixed 358 mm distance between the laser tip and substrate for single-layer, single-pass cladding. However, laser power (P), scanning speed (v), and overlap percentage (OL%) are considered the main parameters in this study. To better characterize the cladding process, specific energy (Es) is calculated using equation (1), where Es is in J/mm³, P in W, d in mm², and v in mm/s as it provides a more detailed index of process efficiency. Given the fixed spot size area of the laser beam approximately around 16 mm², variations in Es directly influence the microstructure and amorphous content of the FeCrMoCB metallic glass (MG) coating layer. **Table 1** shows the LC parameters, where laser power was limited to 250–300 W, and scanning speed was set at 50–70 mm/s, achieving uniform coatings with strong metallurgical bonding. The Taguchi method was employed to design the parameter combinations and reduce the total number of experimental runs.

$$E_S = \frac{P}{d \times v}$$
....(Equation 1)

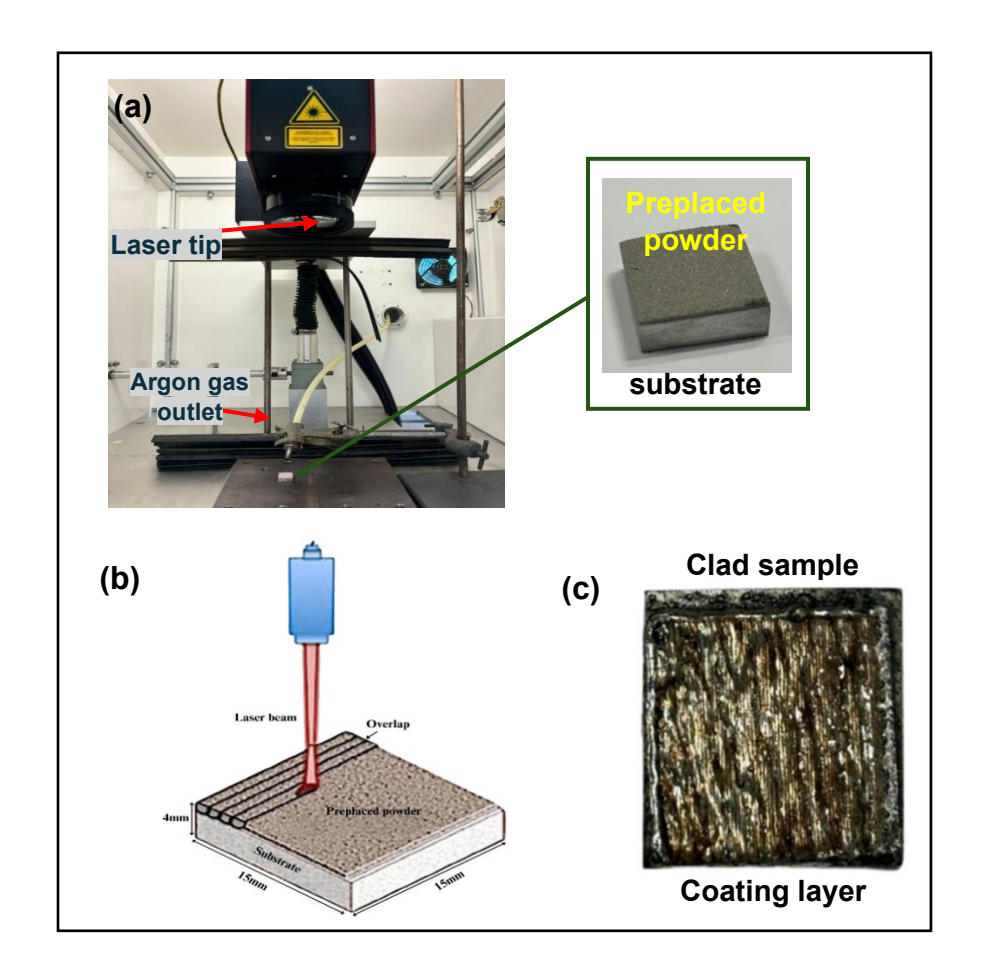


Figure 1: (a) LC configuration, (b) laser scanning orientation and (c) post-coating visual representation

Table 1: The experimental parameters of LC

Sample	Laser power, W	Scanning speed, mm/s	OL %	E, J/mm ³
S1	250	50	30	0.3125
S2	250	60	40	0.2604
S3	250	70	50	0.2232
S4	280	50	40	0.3500
S5	280	60	50	0.2917
S6	280	70	30	0.2500
S7	300	50	50	0.3750
S8	300	60	30	0.3125
S9	300	70	40	0.2679

2.3 Wear Testing setup

Wear resistance was evaluated under dry and grease conditions utilizing a High-Frequency Reciprocating Rig (HFRR) wear tester, as depicted in Figure 2. These testing conditions were selected to simulate the diverse operating environments encountered by tribological components in real-world applications, such as those found in automotive and industrial machinery. In such systems, components often experience both unlubricated and lubricated regimes due to intermittent lubrication, contamination, or varying operating conditions [18], [19]. Before conducting the tests, all nine coating samples were polished until a mirror quality was achieved, and the roughness of all coating specimens was similar to that of uncoated polished steel. The wear tests were performed in lubricated as well as dry configurations as mentioned in Table 2. The counterbody material and testing conditions were selected to mimic operational loads and sliding interactions found in reciprocating tribological systems. This enables direct analysis of coating durability and wear mechanisms under practical conditions. The lubricant used was about 0.2 grams of mineral oil-based automotive grease (NLGI 3) applied to the samples. NLGI 3 grease is thicker, therefore it won't run out and provides lasting lubrication even in high pressure and movement.

Wear and friction coefficient results were collected to assess performance. The wear rate of the fabricated samples and bare substrate was calculated by using equation (2), where Wr represent the wear rate (mm³/N.m), V_{loss} depicts the volume loss in mm³ ($V_{loss} = (m_{before} - m_{after})/\rho$), D demonstrates the total sliding distance (m), and F signifies the applied normal load (N). This approach mirrors the conditions used in recent studies to compare wear performance across different environments [20]. Testing of dry and grease-lubricated conditions was carried out. The specific parameters for the wear tests are shown in Table 2. To ensure reliability and repeatability, each tribological test (both COF and

wear rate) was conducted in triplicate (n = 3) for all coated and uncoated samples. The average values and standard error (SE) were calculated and are summarized in Table 3 and 4. These values were used to generate the corresponding plots in Figures 8, 9, 12, and 13, with error bars representing \pm one standard deviation (SE). After the wear tests, the wear tracks on all coated samples were examined using Optical Microscopy (OM) to evaluate surface wear morphology. A Motic Panthera digital optical microscope was used to capture images at a calibrated magnification with a scale of 200 μ m, ensuring consistent comparison across all samples.

$$W_r = \frac{V_{loss}}{D \times F}$$
 (Equation 2)

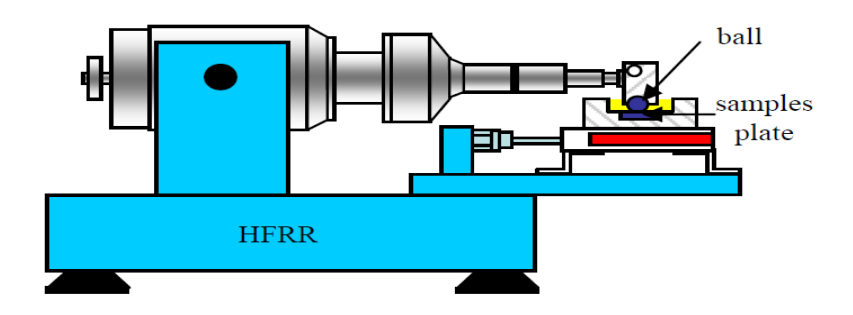


Figure 2: Schematic presentation of High-Frequency Reciprocating Rig (HFRR) wear tester setup

Table 2: Wear test conditions

Sliding condition	Dry	Lubricated		
Load (N)	5	10		
Room temperature (°c)	Room temp.	Room temp.		
Sliding speed (m/s)	0.2	0.2		
Stroke length (mm)	8	8		
Sliding distance (m)	576	576		
Friction time (minutes)	60	60		

2.4 Characterization Methods

Full characterization of the microstructure, compositions, and mechanical properties, as linked to the wear resistance of laser-clad Fe-based amorphous coatings, was carried out. For Optical Microscope (OM), Scanning Electron Microscopy (SEM) [21] and X-ray Diffraction (XRD) [22], an analysis of the surface morphology and microstructure of the laser-clad Fe-based coatings was performed. Metallographic preparation of fabricated samples for cross-sectional examination involved polishing with sandpaper and diamond powder until a scratch-free mirror-like surface was obtained. Afterwards, it was chemically etched in Linsenätzmittel solution (70 mL HCl, 1000 mL ethanol, 40 g FeCl₃, and 30 g CuCl₂) for 1 minute. The microstructure of the coating layer (CL) was investigated through the use of

SEM analysis. In contrast, the coating crystallinity was analyzed by X-ray diffraction (Japan, Rigaku, Miniflex, XRD) with Cu K α radiation (λ = 0.1541 nm). Amorphous materials scatter into diffuse rather than distinct diffraction peaks without long-range atomic order. The phases and microstructures of the laser-clad Fe-based alloy coatings were analysed using Energy Dispersive X-ray spectroscopy (EDS) attached to a scanning electron microscope (SEM, Phenom XL Desktop). In addition, the Vickers microhardness tester (HV-1000, FALCON450G2) was employed to measure microhardness on cross-sections and afterwards coated surfaces with a 10 kgf force with a 10-second dwell time. Microhardness was analyzed at three points on each CL surface, and the average was computed. Such methods allow for extensive examination of the coating's microstructural features and mechanical stability, known as critical parameters which affect their performance in reciprocating wear applications [23], [24].

3.0 Results

116

117

118

119

120

121

122

123

124

125

126

127

128

129

130

131

132

133

134

135

136

137

138

139

140

141

142

143

3.1 Coating Microstructure and Composition

The microstructure and phase composition of laser-clad Fe-based amorphous coatings were analyzed to assess their characteristics and the quality of the laser-cladding process. Figure 3 presents SEM images of the cross-section, showing a uniform microstructure with minimal porosity and a high degree of amorphous phase content. Figure 4 illustrates the clear EDS-mapping of Fe, Cr, Mo, C and B distributions enhances understanding of phase separation, as also observed in recent coating studies [25]. Since all coatings exhibited similar elemental distribution patterns, only the mapping result for coating S6 is shown as a representative example. Microstructural analysis revealed dendritic and equiaxed grain formations, particularly in regions where the amorphous phase partially crystallized. These microstructural changes may influence the coating's mechanical properties, particularly hardness and wear resistance. Zhang et al. demonstrated that laser cladding could produce high-quality Fe-based coating for industry applications in terms of microstructural properties [26]. The X-ray Diffraction (XRD) showed the presence of both amorphous and crystalline phases, with Fe, Cr, and Mo as primary elements. XRD patterns in Figure 5 confirm the phase composition and reveal the presence of C, Fe-Cr, Fe₂₃B₆, Fe, and Fe₃C phases, showing characteristic amorphous peaks alongside crystalline features. The amorphous structure is essential for enhancing wear resistance due to its high hardness and uniformity, as noted in recent studies [27]. The presence of a distinct XRD peak around 30° in samples S3, S5, S6, S8, and S9 suggests the formation of carbon-related phases, which are commonly observed in Fe-C-based alloys due to phase transformations influenced by alloy composition, heat treatment, and carbide precipitation. Additionally, the presence of carbon or iron-chromium

carbide phases in these samples can be attributed to the diffusion of carbon and chromium during thermal processing, leading to carbide stabilization and peak intensity variations in XRD patterns [28]. Similar findings have been reported in Fe-based alloys, where the precipitation of cementite and chromium carbides significantly alters the microstructural properties and diffraction behavior [29]. The presence of amorphous regions was inferred from the broad halo peaks in XRD spectra, consistent with findings in similar Fe-based systems [30]. Further analysis via Raman or XPS could enhance phase resolution and will be explored in future work.

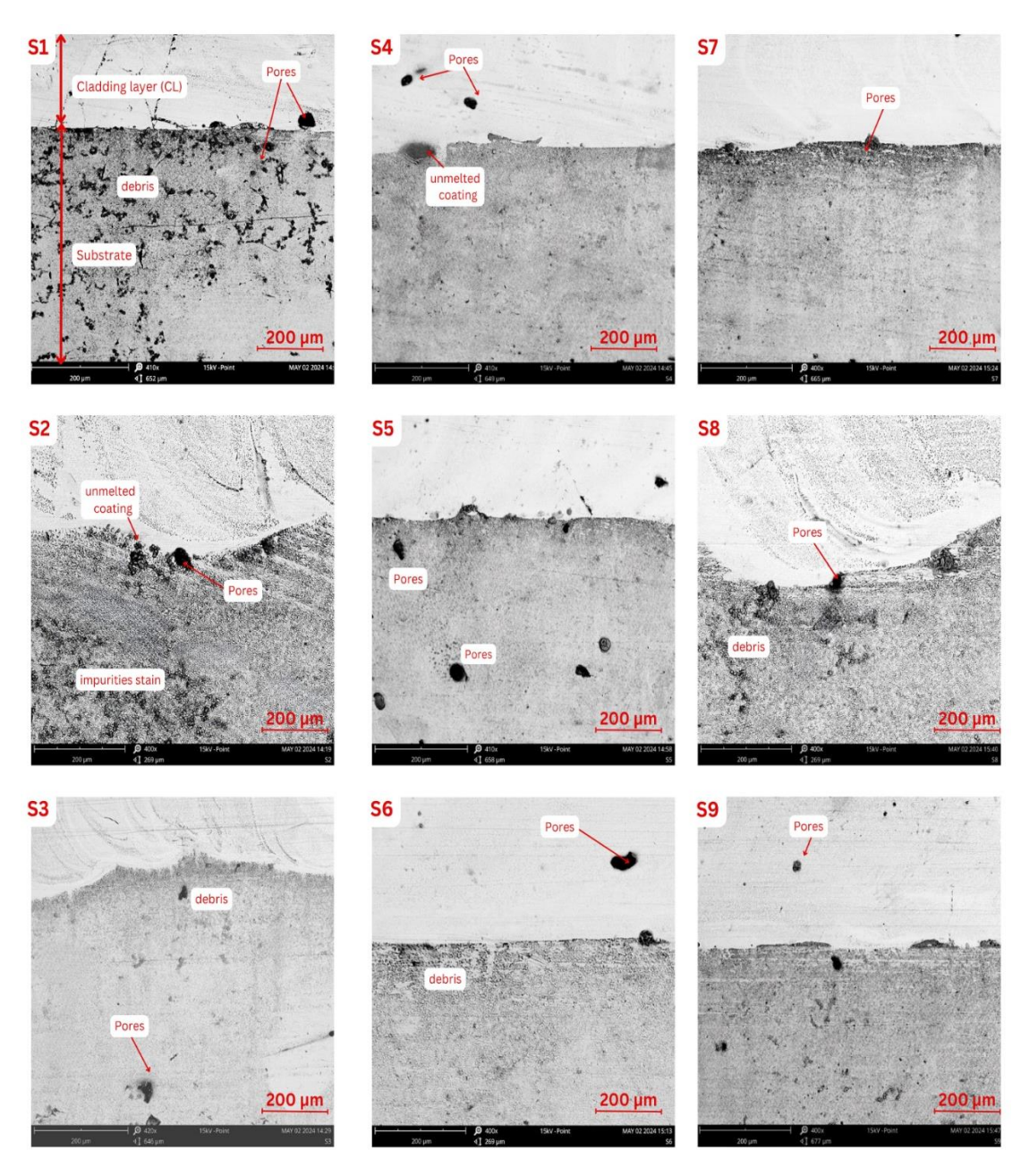


Figure 3: SEM morphology microstructure with scale 200 μm of fabricated samples.

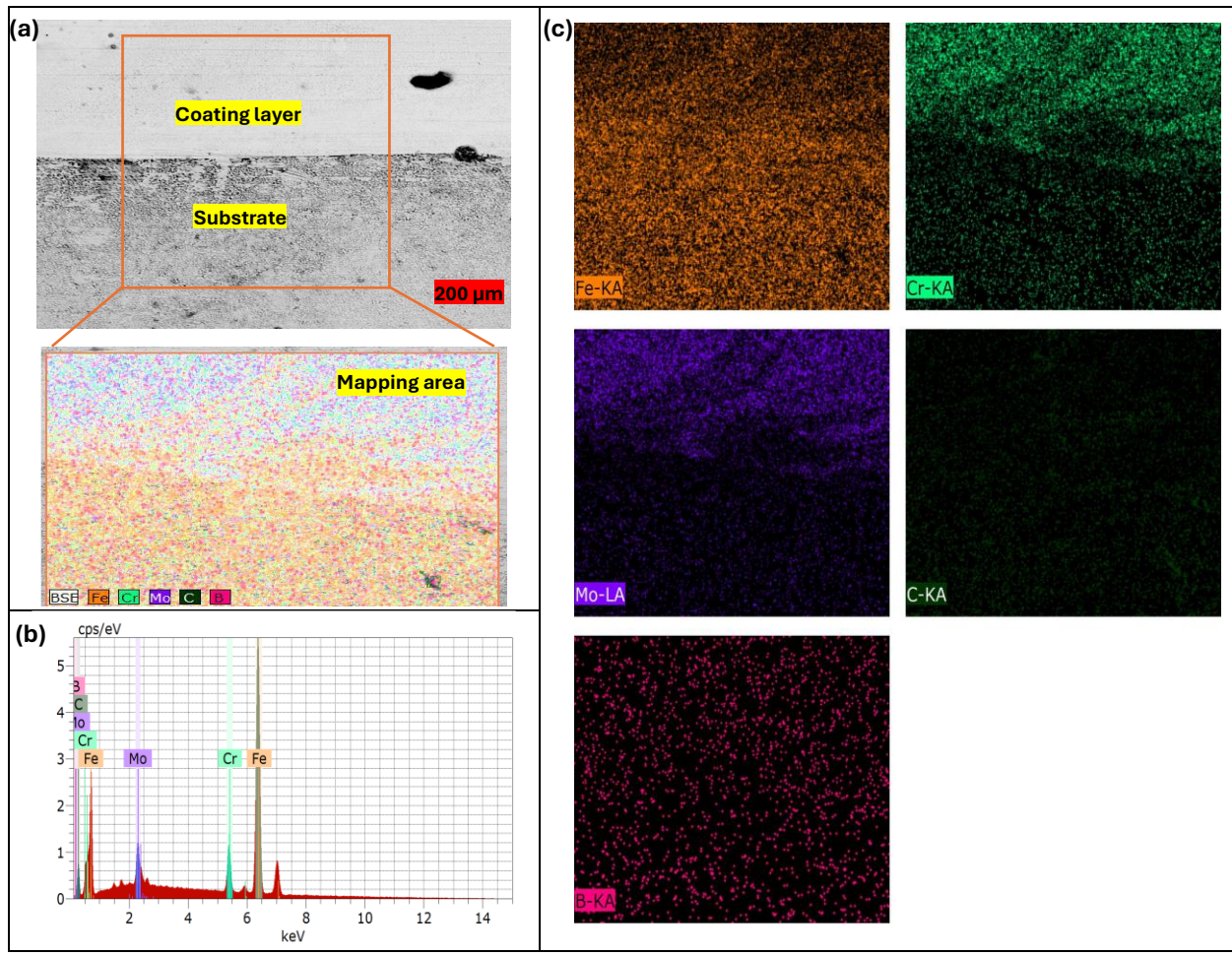


Figure 4: (a) SEM and EDS mapping showing the coated layer and substrate of S6 with micrograph scale (200 μm),

(b) Elemental analysis of samples mapping (S6) and (c) Elemental distribution based on colour coding of EDS mapping.

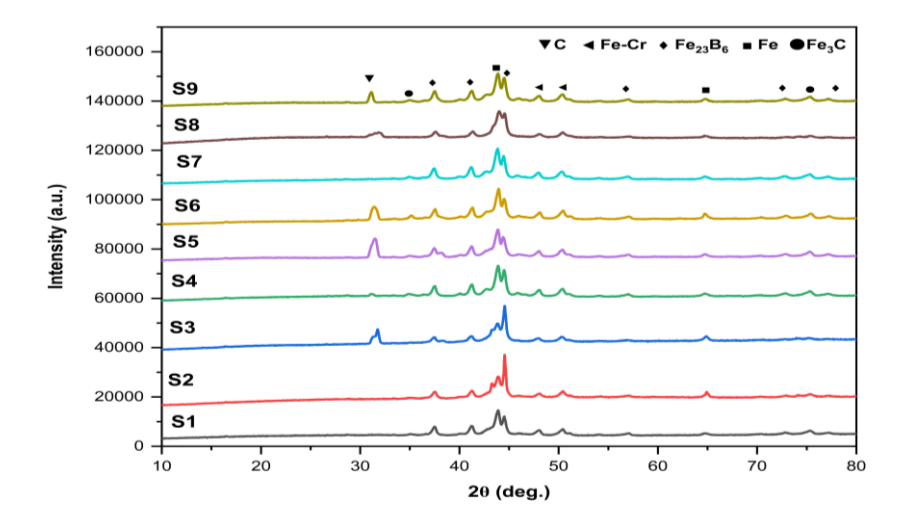


Figure 5: XRD pattern of all nine coated samples.

3.2 Mechanical Properties

The wear-resistant mechanical properties of the coating, specifically hardness was evaluated. The hardness profile across the coating thickness, shown in Figure 6 (a), demonstrates consistently high hardness values around 1100 HV, significantly exceeding that of the AISI 52100 steel substrate. Figure 6(b) compares the microhardness at different levels on the coating surface, confirming that the Fe-based amorphous phase is the primary contributor to mechanical strength. The coating exhibits exceptionally high hardness, attributed to the deformation resistance of the Fe-based amorphous phase and its superior wear resistance compared to conventional crystalline structures [31]. Fine equiaxed grains in the amorphous regions further enhance hardness by minimizing grain boundary defects, thereby improving mechanical performance. Studies widely confirm that these microstructural features enhance hardness and wear resistance, making laser-clad coatings well-suited for high-load applications in demanding environments [32].

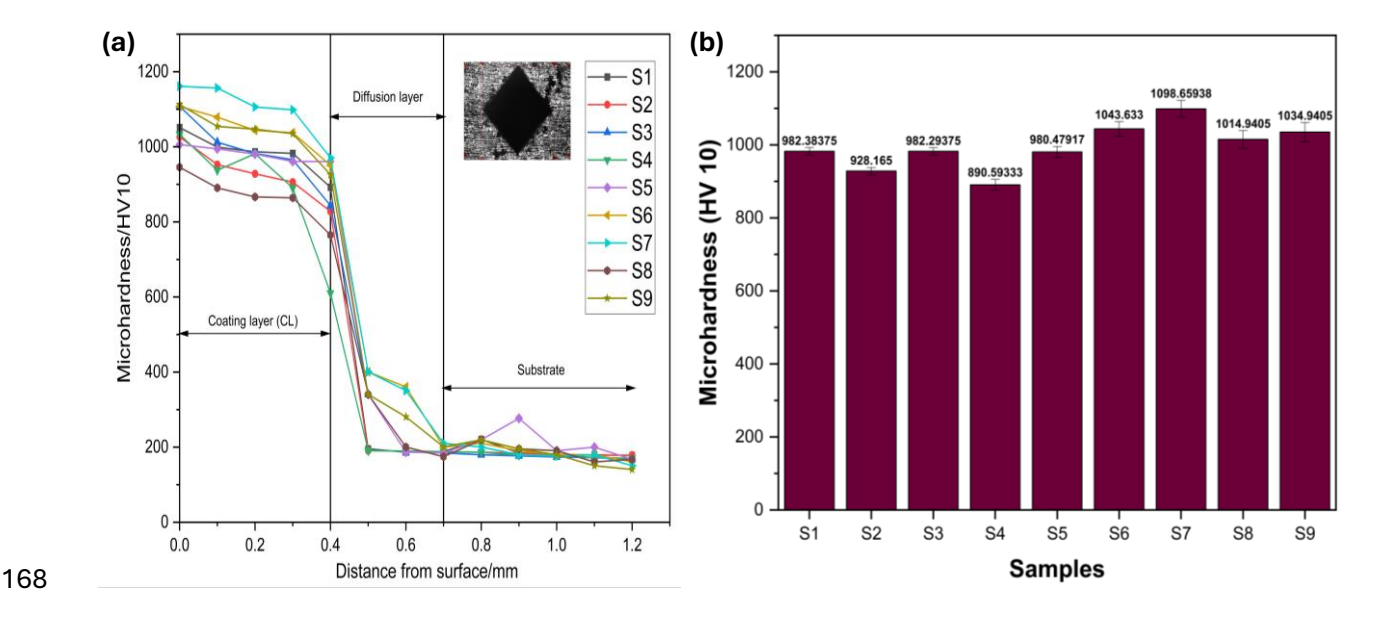


Figure 6: Microhardness values of fabricated samples (a) Cross section and (b) Profile surface.

3.3 Wear Resistance under Dry Conditions

Wear tests in dry conditions were performed to provide a baseline wear resistance value for the laser-clad coatings without the effect of lubricants. Figure 7 presents OM images of the wear tracks, showing a smooth surface with minimal abrasive wear marks, indicating lower material loss. In Figure 7, even though the HFRR stroke length was kept constant at 8 mm, the wear track widths and lengths vary significantly. This variation is attributed to differences in coating hardness, surface microstructure, and frictional interaction factors known to influence wear scar geometry

in dry sliding conditions [33]. As shown in Table 3, the tribological performance of the coated samples exhibits consistent results across all three test runs. The inclusion of standard error quantifies the variability, supporting the trends shown in the subsequent graphs where error bars are used. Figure 8 plots the friction coefficient over time under dry sliding conditions, demonstrating stable frictional behavior. This stability further supports the coating's high wear resistance, even in the absence of lubrication. Among all tested samples, S6 and S7 demonstrated the best wear resistance. As shown in Figure 8(a), they exhibited the lowest average coefficients of friction (COF), with S6 at approximately 0.138 and S7 at 0.167. Figure 8(b) further illustrates their stable COF profiles across different sliding distances. This low friction performance is complemented by their minimal wear volume loss in Figure 9, with S6 at wear rates of 2.222 × 10⁻⁸ mm³/N·m and 3.334 × 10⁻⁸ mm³/N·m for S7.

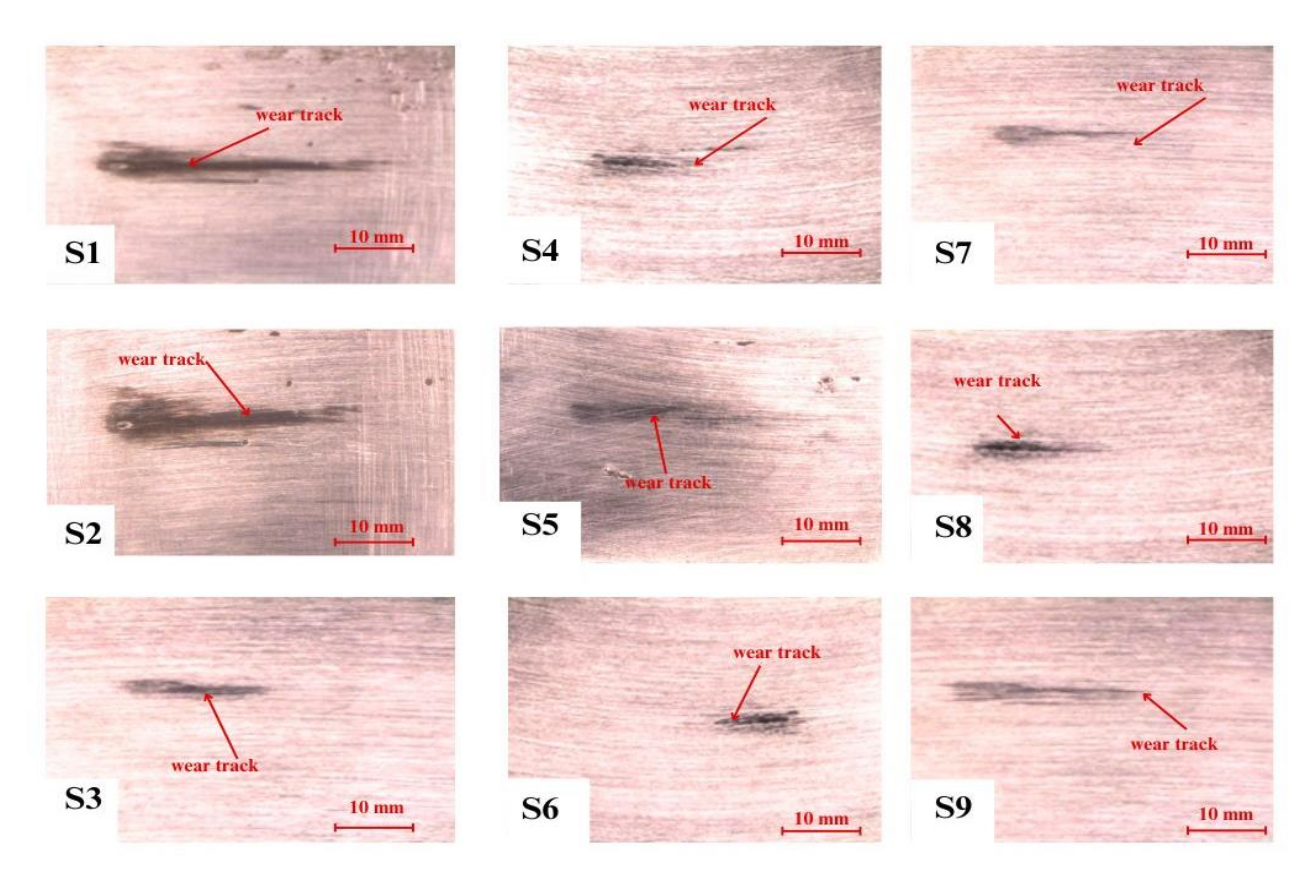


Figure 7: Microscopic images of wear tracks (50× magnification) of fabricated samples under dry conditions.

Samples S6 and S7 demonstrated the lowest mean COF and wear rates with minimal variation, confirming their superior performance. The inclusion of standard error quantifies the variability, supporting the trends shown in the subsequent graphs where error bars are used. These results indicate that S6 and S7 are the most effective in minimizing wear and friction, making them promising candidates for applications that require high durability and reduced friction

in dry environments. Figure 10 illustrates the wear damage mechanisms in sample S6, which was identified as the optimized sample due to its superior performance under dry conditions with load 5 N. The figure 10(a) schematic highlights the formation of cracks and debris, with S6 demonstrating enhanced resistance attributed to its protective crystalline layers. In comparison, the laser-clad coatings exhibited significantly lower wear rates than uncoated AISI 52100 steel, which showed severe wear and surface damage under identical conditions. This enhanced performance aligns with findings from recent studies, which report that Fe-based amorphous coatings produced by laser cladding possess excellent wear resistance in dry conditions due to their hardness and uniform microstructure [10].

Table 3: Average Coefficient of Friction (COF) under dry condition and Wear Rate of Uncoated and Coated Steel Samples with Standard Error (SE).

Samples	Average COF				Wear Rate (mm³/N.m)			
	Test 1	Test 2	Test 3	Mean ± SE	Test 1	Test 2	Test 3	Mean ± SE
Uncoated Polished Steel	0.2118	0.2118	0.2100	$\begin{array}{c} 0.2112 \pm \\ 0.0006 \end{array}$	1.11×10 ⁻⁷	1.91×10 ⁻⁷	1.91×10 ⁻⁷	$1.64 \times 10^{-7} \pm 2.67 \times 10^{-7}$
S1	0.1852	0.1872	0.1909	$\begin{array}{c} 0.1877 \pm \\ 0.0016 \end{array}$	3.33×10 ⁻⁸	4.43×10 ⁻⁸	4.44×10 ⁻⁸	$4.07 \times 10^{-8} \pm 3.68 \times 10^{-9}$
S2	0.1717	0.1717	0.1817	0.1751 ± 0.0033	6.67×10 ⁻⁸	7.07×10 ⁻⁸	7.08×10 ⁻⁸	$6.94 \times 10^{-8} \pm 1.35 \times 10^{-9}$
S3	0.1775	0.1875	0.1771	$\begin{array}{c} 0.1807 \pm \\ 0.0034 \end{array}$	8.89×10 ⁻⁸	8.90×10 ⁻⁸	8.93×10 ⁻⁸	$8.91 \times 10^{-8} \pm 1.25 \times 10^{-10}$
S4	0.1815	0.1894	0.1913	$\begin{array}{c} 0.1874 \pm \\ 0.0030 \end{array}$	3.78×10 ⁻⁸	3.87×10 ⁻⁸	3.96×10 ⁻⁸	$3.87 \times 10^{-8} \pm 5.19 \times 10^{-10}$
S5	0.1737	0.1747	0.1847	0.1777 ± 0.0035	4.45×10 ⁻⁸	4.49×10 ⁻⁸	4.53×10 ⁻⁸	$4.49 \times 10^{-8} \pm 2.31 \times 10^{-10}$
S6	0.1312	0.141	0.1421	$\begin{array}{c} 0.1381 \pm \\ 0.0034 \end{array}$	2.22×10 ⁻⁸	2.25×10 ⁻⁸	2.27×10 ⁻⁸	$\begin{array}{c} 2.25 \times 10^{-8} \pm \\ 1.28 \times 10^{-10} \end{array}$
S 7	0.1634	0.1654	0.1738	0.1675 ± 0.0032	3.33×10 ⁻⁸	3.34×10 ⁻⁸	3.35×10 ⁻⁸	$3.34 \times 10^{-8} \pm 5.09 \times 10^{-11}$
S8	0.1688	0.1717	0.1697	$\begin{array}{c} 0.1701 \pm \\ 0.0008 \end{array}$	6.67×10 ⁻⁸	6.84×10 ⁻⁸	6.90×10 ⁻⁸	$6.80 \times 10^{-8} \pm \\ 6.94 \times 10^{-10}$
S9	0.1711	0.1811	0.1710	0.1744 ± 0.0033	6.67×10 ⁻⁸	6.84×10 ⁻⁸	7.00×10 ⁻⁸	$6.84 \times 10^{-8} \pm 9.62 \times 10^{-10}$

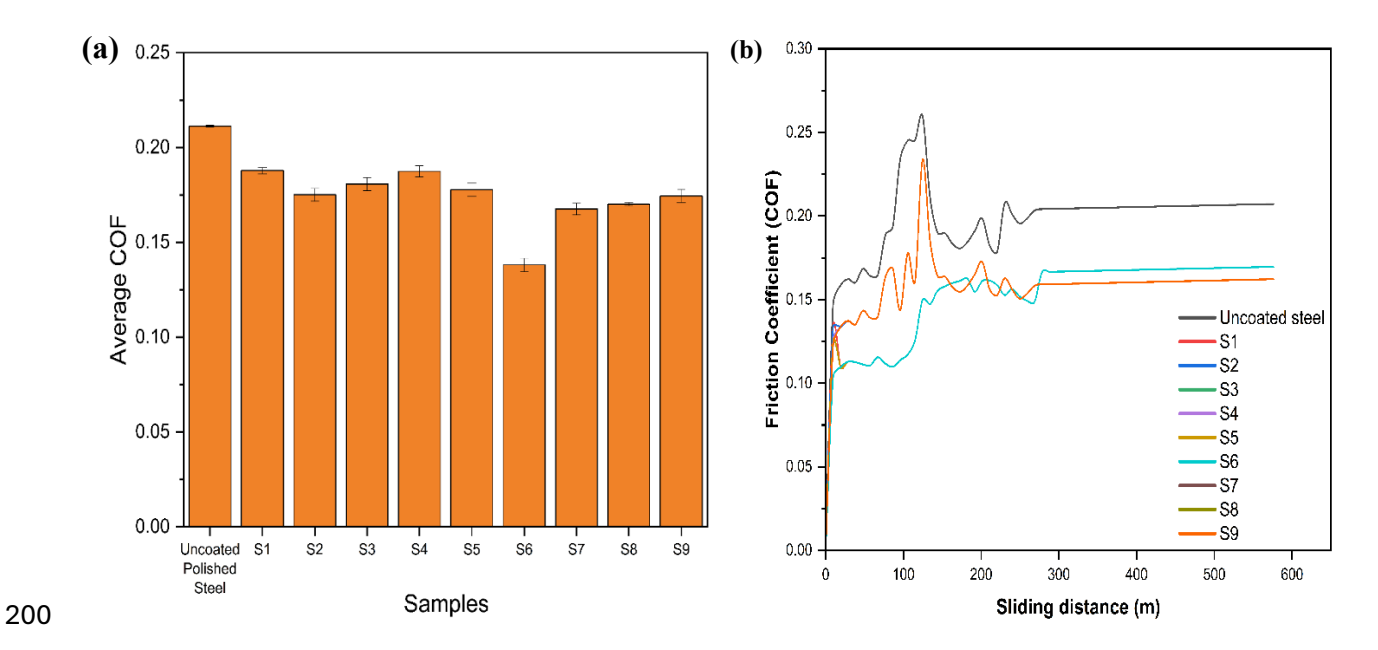


Figure 8: Tribological results for polished steel and fabricated samples under dry sliding conditions: (a) Average COF; (b) the change of COF with sliding distance for the coatings.

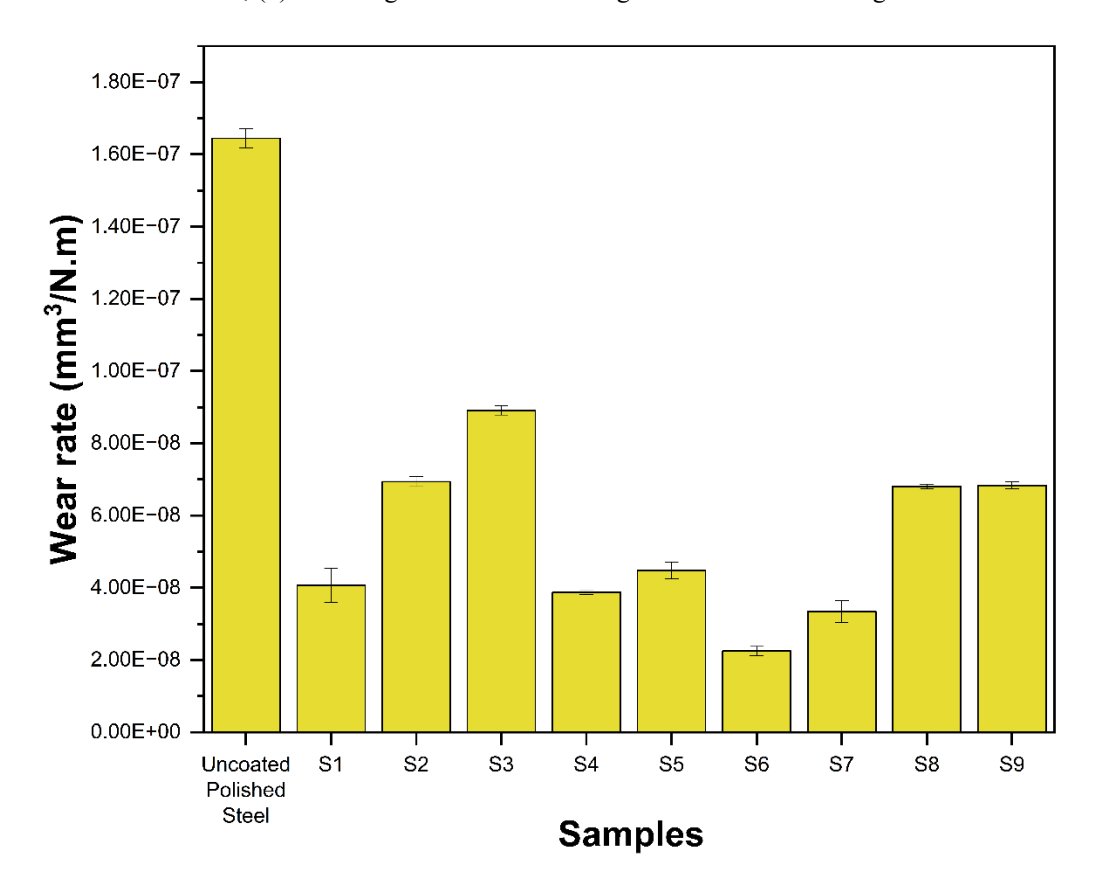


Figure 9: Tribological results (wear rate) for polished steel and fabricated samples under dry sliding conditions.

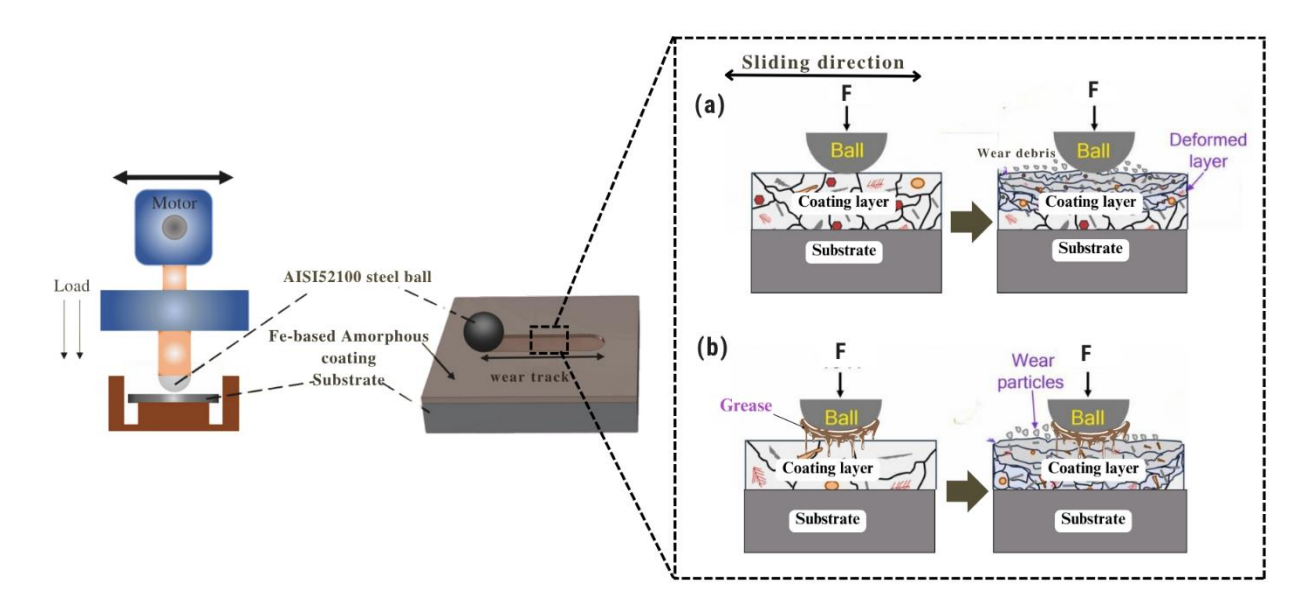


Figure 10: Schematic diagram showing the wear damage mechanism with different condition in fabricated samples S6: (a) dry (with load 5N) and (b) grease lubricated condition (with load 10N).

3.4 Wear Resistance under Grease-Lubricated Conditions

Wear performance under lubricated conditions was evaluated using lithium-based grease as a lubricant. Grease lubrication significantly reduced the coefficient of friction (COF), leading to lower material loss and a smoother wear track [26]. This enhancement in wear performance was evident across all samples, with further improvements in surface quality and friction stability. Figure 11 presents optical microscopic images of the wear track, revealing a smoother surface compared to dry conditions, with minimal abrasive features and reduced surface roughness. From the figure 11, the grease-lubricated wear tracks also display non-uniform lengths and widths, which can be attributed to localized formation of protective tribofilms and variation in contact stress distribution, factors known to influence wear scar geometry under boundary-lubricated regimes [34]. As shown in Table 4, the tribological performance of the coated samples under grease-lubricated condition exhibits consistent results across all three test runs. The inclusion of standard error quantifies the variability, supporting the trends shown in the subsequent graphs where error bars are used. Additionally, the friction coefficient 7000 lower values and reduced fluctuation, indicating the beneficial impact of lubrication on wear resistance. Therefore, under grease-lubricated conditions, samples S6 and S7 demonstrated superior wear resistance, as indicated by their low coefficients of friction (COF) and narrower wear tracks. Specifically, S6 and S7 achieved COF values of 0.104 and 0.107, respectively, ranking among the lowest across all samples (Figure 12a).

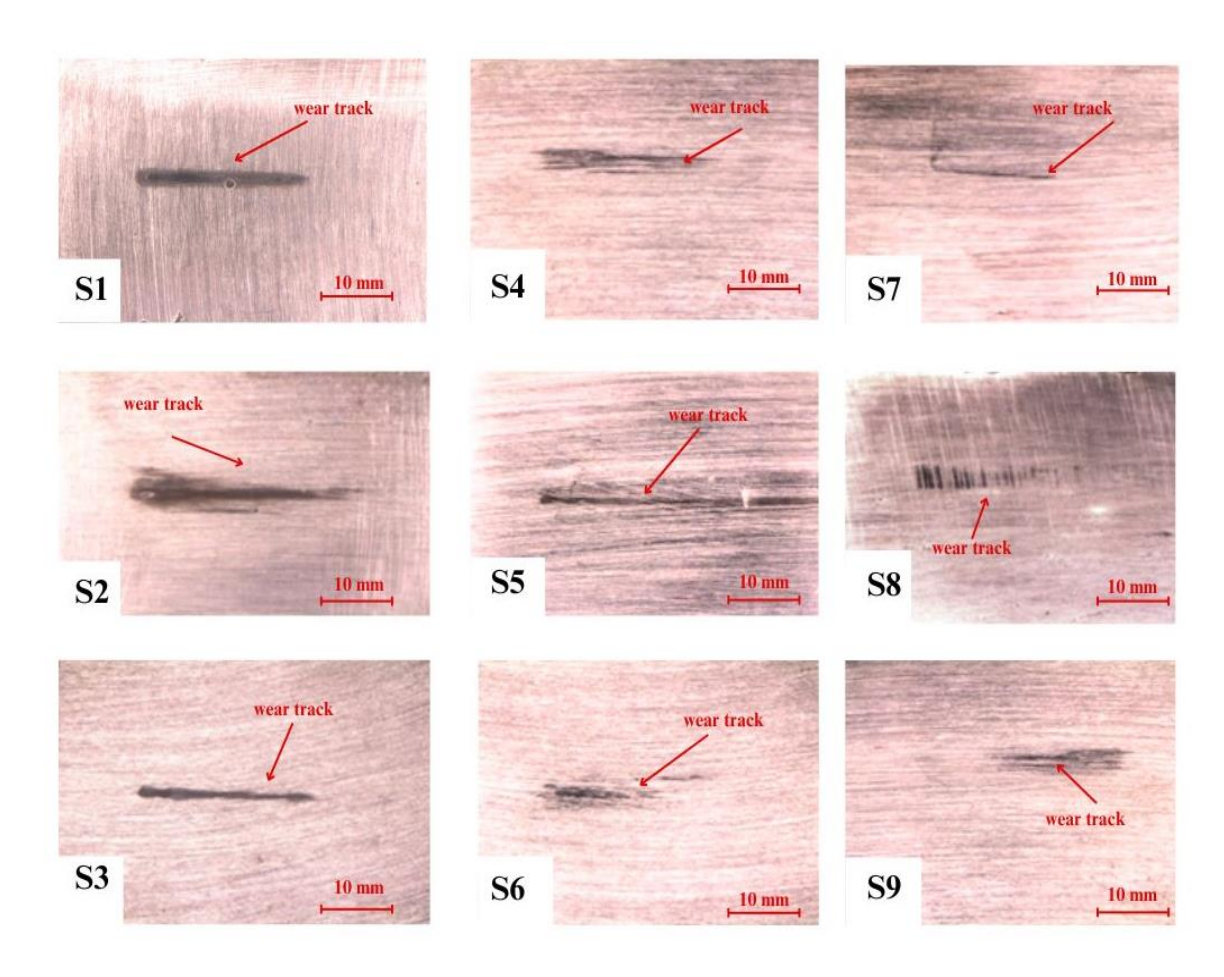


Figure 11: Microscopic images of wear tracks (50× magnification) of fabricated samples under lubricated conditions.

Figure 13 illustrates that S6 recorded the lowest wear volume loss at 0.000012 mm³ and a wear rate of 2.22×10^{-8} mm³/N·m, followed closely by S7 with a wear volume loss of 0.000019 mm³, including a wear rate of 3.33×10^{-8} mm³/N·m. These values are significantly lower than other samples, making S6 and S7 the most effective in reducing material loss under lubricated conditions. This combination of low COF, minimal wear volume loss, and low wear rate highlights their suitability for applications requiring enhanced wear resistance. Surface analysis of the wear track revealed minimal abrasive wear patterns and the absence of adhesive wear. This suggests that grease lubrication effectively reduced direct metal-to-metal contact, thereby improving the coating's resistance to sliding wear. These findings align with previous studies, which report that lubrication substantially reduces wear rates in Fe-based amorphous coatings by minimizing friction and wear debris formation[35], [36].

Table 4: Average Coefficient of Friction (COF) under lubricated condition and Wear Rate of Uncoated and Coated Steel Samples with Standard Error (SE).

	Average COF				Wear Rate (mm ³ /N.m)			
Samples	Test 1	Test 2	Test 3	Mean ± SE	Test 1	Test 2	Test 3	Mean ± SE
Uncoated Polished Steel	0.13173	0.13099	0.12999	0.1309 ± 0.0005	1.56×10 ⁻⁷	1.57×10 ⁻⁷	1.59×10 ⁻⁷	$1.57 \times 10^{-7} \pm 8.98 \times 10^{-10}$
S 1	0.11162	0.1125	0.1098	0.1113 ± 0.0008	4.45×10 ⁻⁸	4.89×10 ⁻⁸	5.34×10 ⁻⁸	$4.89 \times 10^{-8} \pm 2.57 \times 10^{-9}$
S2	0.11262	0.102	0.1099	0.1082 ± 0.0032	6.67×10 ⁻⁸	6.84×10 ⁻⁸	7.00×10 ⁻⁸	$6.84\times10^{-8}\pm9.62\times10^{-10}$
S3	0.12062	0.11995	0.1225	0.1210 ± 0.0007	8.89×10 ⁻⁸	9.18×10 ⁻⁸	9.47×10 ⁻⁸	9.18×10 ⁻⁸ ± 1.67×10 ⁻⁹
S4	0.11252	0.11195	0.10991	0.1115 ± 0.0007	6.67×10 ⁻⁸	6.80×10 ⁻⁸	6.92×10 ⁻⁸	$6.80 \times 10^{-8} \pm 7.31 \times 10^{-10}$
S5	0.11142	0.11442	0.11052	0.1121 ± 0.0012	1.33×10 ⁻⁷	1.46×10 ⁻⁷	1.58×10 ⁻⁷	$1.46 \times 10^{-7} \pm 7.01 \times 10^{-9}$
S 6	0.10589	0.104	0.103	0.1043 ± 0.0009	2.22×10 ⁻⁸	2.35×10 ⁻⁸	2.47×10 ⁻⁸	$2.35 \times 10^{-8} \pm 7.06 \times 10^{-10}$
S7	0.11138	0.10009	0.112	0.1078 ± 0.0039	3.33×10 ⁻⁸	3.37×10 ⁻⁸	3.40×10 ⁻⁸	$3.37 \times 10^{-8} \pm 1.93 \times 10^{-10}$
S8	0.1121	0.111	0.1131	0.1121 ± 0.0006	1.11×10 ⁻⁷	1.12×10 ⁻⁷	1.13×10 ⁻⁷	$1.12 \times 10^{-7} \pm 6.42 \times 10^{-10}$
S9	0.1114	0.1121	0.1105	$\begin{array}{c} 0.1113 \pm \\ 0.0004 \end{array}$	4.45×10 ⁻⁸	4.59×10 ⁻⁸	4.73×10 ⁻⁸	$4.59 \times 10^{-8} \pm 8.34 \times 10^{-10}$



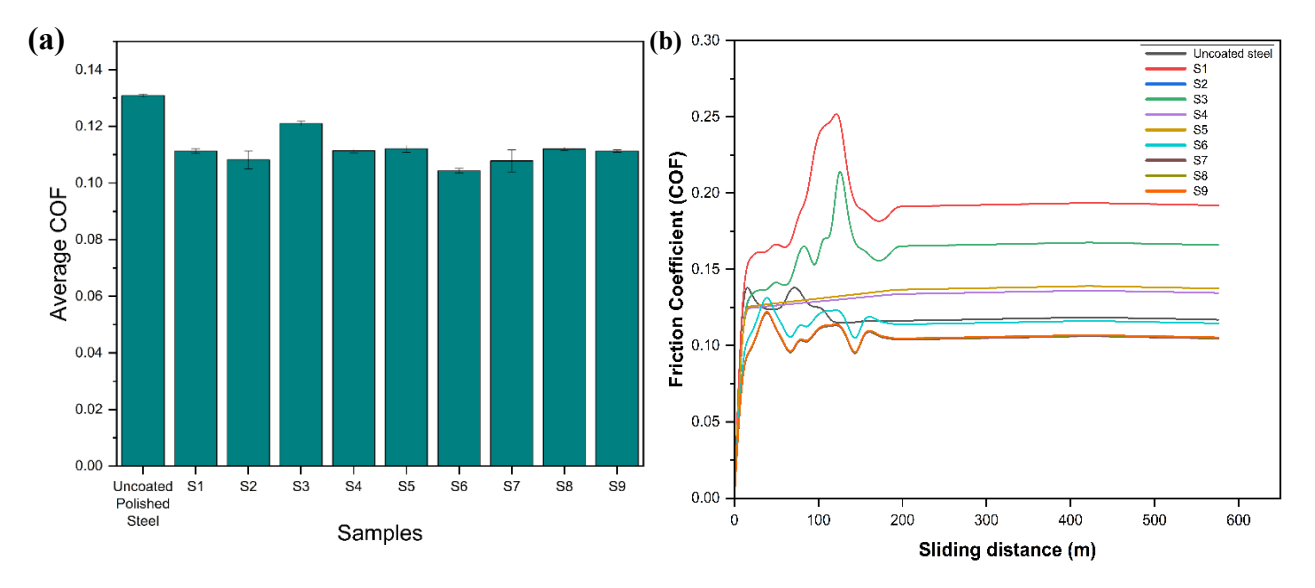


Figure 12: Tribological results for polished steel and fabricated samples under lubricated sliding conditions: (a)

Average COF; (b) the change of COF with sliding distance for the coatings.

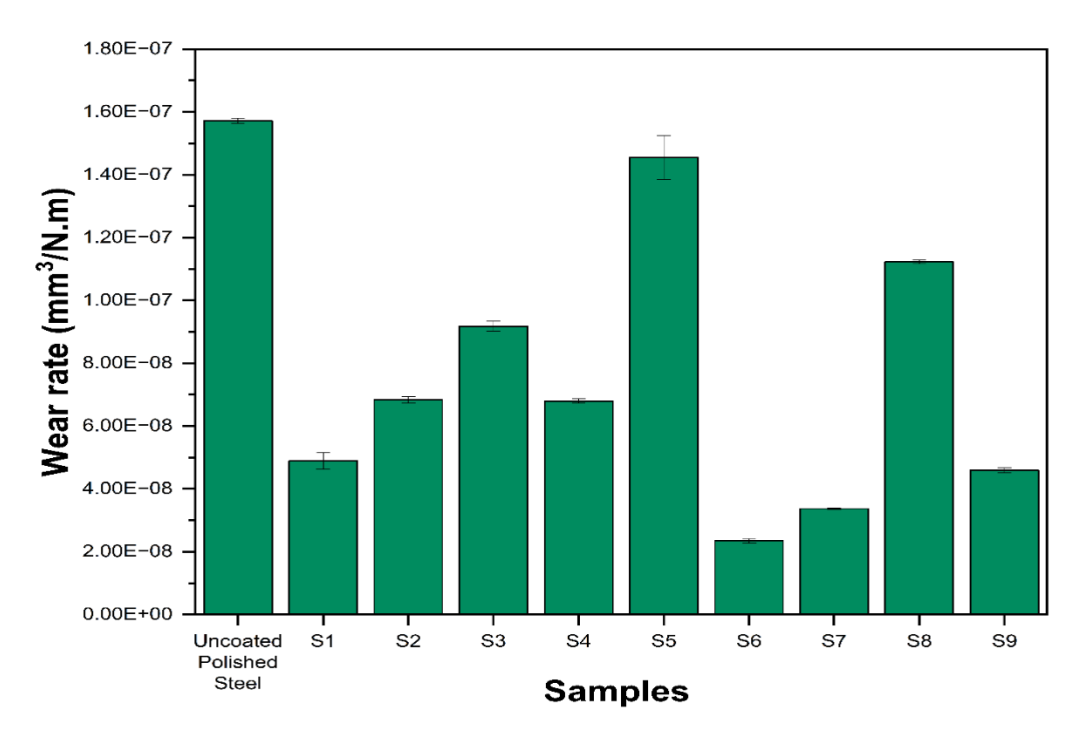


Figure 13: Tribological results (wear rate) for polished steel and fabricated samples under lubricated sliding conditions.

Thus, the schematic diagram in Figure 10(b) illustrates the wear damage mechanisms for samples S6 under grease-lubricated conditions with load 10 N, emphasizing the interaction between the ball and the surface coatings. For Sample S6, the wear track is characterized by pronounced cracks and debris formation, indicating abrasive wear and coating delamination as dominant mechanisms. This highlight the critical role of coating microstructure and composition in mitigating wear under lubricated sliding conditions, corroborating findings in recent studies that underline the importance of optimized coatings for durability in high-stress applications [37].

4.0 Discussion

Under dry sliding, the wear tracks display prominent abrasive grooves and wear debris, indicating that abrasive wear is dominant, likely combined with localized brittle fracture of the amorphous matrix. This is consistent with the known behavior of Fe-based amorphous coatings, which often fail by micro-cracking and spalling due to their high hardness but limited ductility [38]. Detached particles from these micro-fractures can act as abrasives, intensifying material removal. Moreover, mild adhesive wear may occur at asperity contacts under insufficient lubrication, which can explain the slightly higher COF observed for some coated samples compared to the uncoated steel [39]. Overall, the coating's resistance to oxidation minimizes any significant oxidative wear under the test conditions, aligning with

previous studies of Fe-based amorphous coatings in dry sliding environments consistent with earlier findings on Fe-based coatings under unlubricated loads [40], [41]. In contrast, grease lubrication provided a boundary layer that significantly reduced asperity interactions, minimizing adhesive wear and resulting in smoother tracks [42]. This lubrication effect explains the 30–40% reduction in wear rate observed in samples S6 and S7. For example, when tested under grease-lubricated conditions, the COF values for these samples were further reduced, with S6 achieving a COF of 0.1043 and S7 a COF of 0.1078, representing approximately a 24.5% reduction for S6 and a 35.6% reduction for S7 compared to their dry condition COF values. This comparison highlights that grease lubrication substantially enhances wear resistance by further lowering the friction in already high-performing samples under dry conditions. Grease lubrication significantly reduced wear and friction across all samples, lowering average COF values by approximately 30–40% compared to dry conditions. Under grease-lubricated conditions, COF values were further reduced, with S6 achieving 0.1043 and S7 0.1078. This corresponds to reductions of approximately 24.5% for S6 and 35.6% for S7 compared to their dry-condition values. This comparison highlights the significant role of lubrication in enhancing wear resistance, particularly for high-performing samples in dry conditions.

Furthermore, the wear performance and hardness of the coated samples are strongly linked to their unique microstructural characteristics. The laser-clad FeCrMoCB coatings primarily consist of an amorphous matrix, confirmed by XRD and cross-sectional micrographs, which provides high hardness due to its grain-boundary-free structure. However, this amorphous phase is inherently brittle and can fracture under repeated sliding, releasing small particles that may act as third-body abrasives and locally increase wear if not stabilized [38]. The embedded crystalline phases, including hard intermetallic carbides such as Fe₂C and Fe₂₃B₆, further enhance hardness but can also contribute to brittleness and micro-crack initiation under dry conditions. At the same time, the presence of limited soft and ductile phases or localized residual matrix regions can help absorb deformation energy and reduce superficial fracture, which may explain the improved wear resistance observed in optimized samples like S6 and S7. This balance between hard–brittle and soft–ductile phases has been shown to be critical for controlling both hardness and wear stability in Febased amorphous coatings [41], [43], [44]. Therefore, the improved tribological behavior can be attributed not just to high hardness but to a microstructure that combines hard phases for load support with localized ductility that limits crack propagation and particle spalling.

Wear volume loss and wear rate were significantly lower under grease lubrication, highlighting the protective role of grease in minimizing material degradation and enhancing overall wear resistance. These findings align with existing literature, which highlights the superior performance of Fe-based amorphous coatings in both dry and lubricated conditions due to their strong adhesion, high hardness, and resistance to abrasive and adhesive wear mechanisms [45]. Under dry sliding conditions, the COF behavior (Figure 14) of several coated samples in this study follows trends observed by Li et al. (2022). Their study reported an initial rise in COF due to direct asperity contact, followed by a steady-state phase [46]. Notably, the coatings developed in this study achieved significantly lower COF values (0.138 for S6 and 0.167 for S7) compared to the 0.404–0.542 range reported by Li et al. (2022).

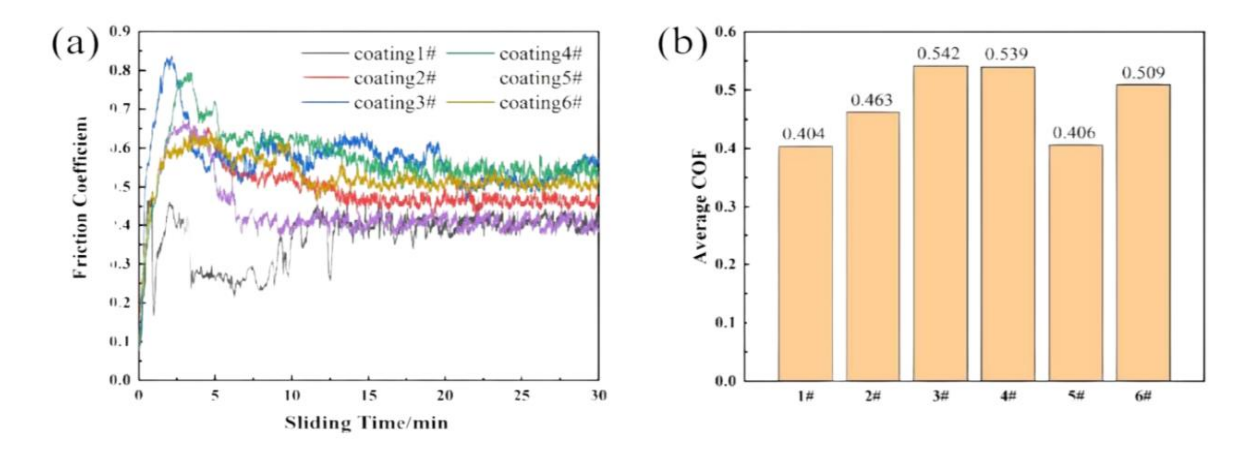


Figure 14: The COF result of the coatings from investigation by Li et al (2022) with fabricated samples under dry sliding condition: (a) the sliding time with change of COF, (b) the average friction coefficient [46].

Figure 7 reveals distinct differences in material wear track loss among the tested samples. This trend aligns with Zhang et al. (2021), who observed reduced wear track lengths in high-hardness coatings under similar test conditions [47]. Conversely, when grease lubrication was used, the wear rate of the coating was further decreased, suggesting that lubrication creates a barrier film that limits frictional contact. The application of NLGI 3 grease provided a thicker lubricating film, preventing direct asperity contact and reducing abrasive wear. Figure 13 highlights this performance enhancement, particularly for S6, which exhibited the lowest wear rate. It can successfully prevent direct metal-to-metal friction/interaction, thus minimizing wear volume and surface roughness in the wear track. This outcome is consistent with studies by Chen et al. (2022), who emphasized the role of lubrication in minimizing adhesive wear and friction [48]. The exact control of the laser parameters during the process, like the power of the laser and the

scanning velocity, made it possible to obtain an amorphous phase that was dense and homogeneous with few defects. Unlike crystalline arrangements of atoms, where defects like grain boundaries and dislocation sites lead to weak points in the material that can allow deformation and wear, amorphous structures are entirely safe from these flaws, making them extremely resistant to deformation and wear [49]. The optimized samples **S6** and **S7** demonstrate excellent wear resistance due to the precise control of laser cladding parameters, including laser power and scanning velocity. As illustrated in the figure 15 [50], SEM micrographs of worn surfaces show that slower scanning speeds produce light grooves and fewer oxide patches, contributing to smoother, less damaged surfaces, whereas faster speeds result in deeper grooves and visible oxide particles that can degrade wear performance investigated by Hou et al. (2019).

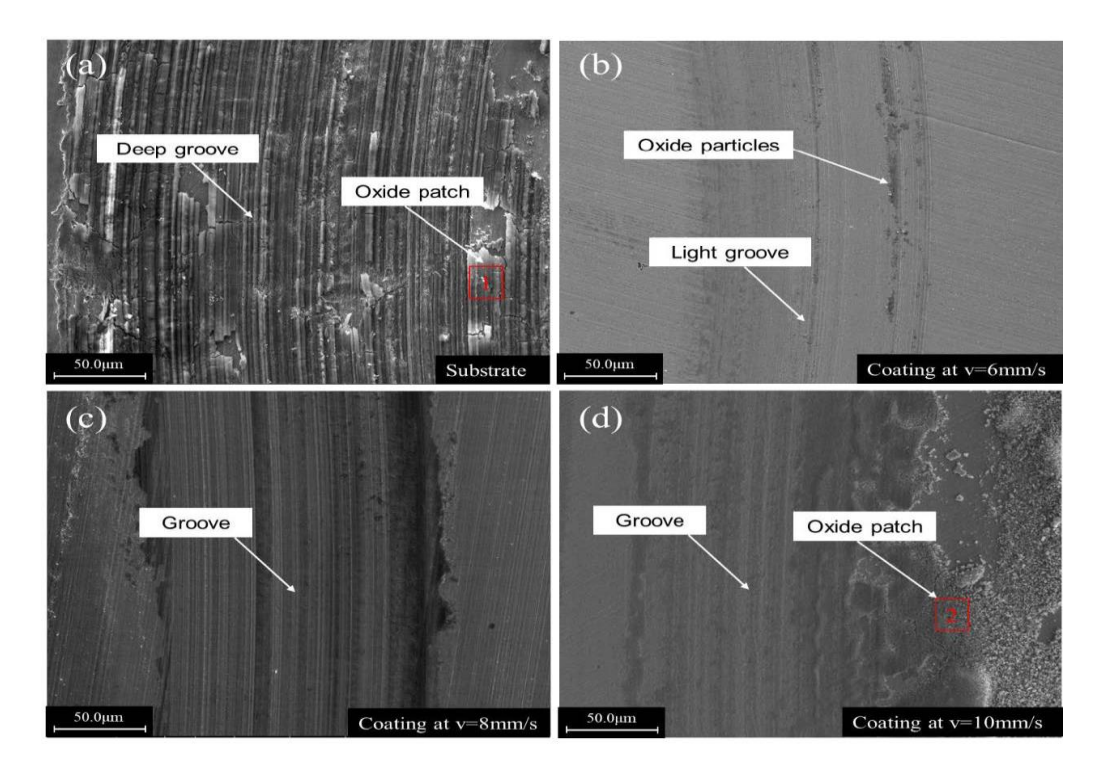


Figure 15: SEM micrographs of the worn surfaces of the substrate and the claddings obtained with different scanning speeds by Hou et al. [50]

This result support previous work on Fe-based amorphous coatings, in particular those produced by laser cladding. For example, Zhang et al. (2022) achieved similar improvements in wear resistance and microhardness for Fe-based coatings manufactured by high-speed laser cladding, attributing these two properties mainly to the absence of grain boundaries in their amorphous structure [51]. Compared to conventional crystalline coatings such as WC–Co and CrN, which typically exhibit wear rates in the range of 3.0×10^{-5} to 6.0×10^{-5} mm³/N·m under dry reciprocating conditions [52],[53], the FeCrMoCB amorphous coating in this study achieved a lower average wear rate of about

1.5 × 10⁻⁷ mm³/N·m. This superior performance is mainly due to its fully amorphous matrix, which eliminates grain boundaries that often act as crack initiation sites under cyclic stress. Furthermore, the presence of Cr and Mo enhances corrosion resistance, while laser cladding ensures excellent metallurgical bonding, enabling higher load-bearing capabilities [54]. These advantages make FeCrMoCB coatings suitable for demanding tribological applications where traditional coatings may fail due to grain boundary oxidation or delamination [55]. In line with the exploration of wear-resistant coatings, Ahmad et al. (2022) demonstrated that optimizing the powder feed rate in plasma-sprayed FeCr-Mo-B-C coatings significantly enhances their microstructural integrity, wear resistance, and corrosion properties, complementing the findings on the performance of laser-clad FeCrMoCB coatings under various lubrication conditions [56]. Further development is needed to tackle these challenges, including the optimization of the coating thickness, the addition of gradient layers, or even hybrid cladding technologies to improve toughness instead of hardness [57]. In conclusion, the current investigation supports the feasibility of utilizing Fe-based amorphous coatings manufactured by laser cladding in high-performance wear applications.

5.0 Conclusion

This study uniquely demonstrates the effectiveness of laser-clad FeCrMoCB amorphous coatings on AISI 52100 steel under both dry and grease-lubricated reciprocating wear conditions, revealing performance improvements not previously reported for this coating–substrate combination. In particular, in Sample S6 and S7, it was found that lubrication resulted in reductions in the coefficient of friction (COF) values of around 24.5% and 35.6%, respectively, which represent general improvements. Furthermore, wear volume loss decreased significantly when lubricated, with both samples showing 30–40% improved wear resistance compared to dry conditions. The considerable improvement with regard to performance can be attributed to the enhanced mechanical properties of the samples, such as the high hardness and structural stability that prevent deformation and mass loss induced and facilitated by friction. Here, the lubrication is either intermittent or can change based on the demand placed on components, specifically in the automotive, aerospace and heavy machinery industries (bearings, gears, etc. Laser cladding of Fe-based semi-amorphous coatings has great potential for lowering the maintenance cost of parts suffering wear, as well as increasing the service life of mission-critical components where the failure implications could justify the cost of laser cladding. Future research could explore multi-layer cladding techniques to further enhance toughness, as well as hybrid coatings that combine amorphous and crystalline phases for improved impact resistance. In summary, this research highlights

- 353 the potential of laser-clad Fe-based coatings to improve component performance in wear-intensive environments. It
- 354 lays the groundwork for advancing durable, wear-resistant materials for industrial use.

355 6.0 References

- T. Coors, Y. Faqiri, F. Saure, F. Pape, T. Hassel, and G. Poll, "Wear of Tailored Forming Steels," *Adv Eng Mater*, vol. 25, no. 13, Jul. 2023, doi: https://10.1002/adem.202201740.
- Z. Peng and K. Dejun, "Microstructure and tribological performances of laser cladded FeCoCrMoSi amorphous coating under different normal loads," *Industrial Lubrication and Tribology*, vol. 77, no. 2, pp. 231–239, Jan. 2025, doi: https://10.1108/ILT-08-2024-0304.
- 361 [3] X. Ji, C. Luo, J. Juan, J. Zhao, and Y. Zhang, "Wear Resistance of Fe-Based Amorphous Powder Deposited Coatings in Air, Water, and SBF Solution: Effect of Layer Number," *Tribology Transactions*, vol. 65, no. 3, pp. 531–541, May 2022, doi: https://10.1080/10402004.2022.2054889.
- 364 [4] H. Han, M. Xiao, and Q. Wang, "Corrosion Performance of Fe-Based Amorphous Coatings via Laser Cladding
 365 Assisted with Ultrasonic in a Simulated Marine Environment," *Metals (Basel)*, vol. 13, no. 12, p. 1938, Nov.
 366 2023, doi: https://10.3390/met13121938.
- C. Han, L. Ma, B. J. Ma, G. Huang, and Y. X. Ma, "The in-situ re-melting post-treatment on properties of atmosphere plasma-sprayed FeCoCrMoCBY amorphous alloy coating," *Anti-Corrosion Methods and Materials*, vol. 70, no. 1, pp. 25–33, Jan. 2023, doi: https://10.1108/ACMM-05-2022-2655.
- Q. Wang *et al.*, "Effect of High-Speed Powder Feeding on Microstructure and Tribological Properties of Fe-Based Coatings by Laser Cladding," *Coatings*, vol. 11, no. 12, p. 1456, Nov. 2021, doi: https://10.3390/coatings11121456.
- Y. Li, Y. Li, W. Wang, M. Lei, and X. Li, "Synthesis Fe-Ni protective coating on 45 steel by laser remelting nickel pre-coating dopped with Fe-based amorphous powders," *Mater Charact*, vol. 176, p. 111129, Jun. 2021, doi: https://10.1016/j.matchar.2021.111129.
- 376 [8] H. Han, M. Xiao, and Q. Wang, "Corrosion Performance of Fe-Based Amorphous Coatings via Laser Cladding
 377 Assisted with Ultrasonic in a Simulated Marine Environment," *Metals (Basel)*, vol. 13, no. 12, p. 1938, Nov.
 378 2023, doi: https://10.3390/met13121938.
- 379 [9] J. Zhang, Y. Wang, Q. Niu, R. Fan, and J. Wu, "Study on toughening of Fe based amorphous coatings by ultra high speed laser cladding," *J Phys Conf Ser*, vol. 2355, no. 1, p. 012075, Oct. 2022, doi: https://10.1088/1742-381 6596/2355/1/012075.
- L. Xie, Y. Wang, J. Yang, C. Li, X. Han, and J. Huang, "MICROSTRUCTURE AND HIGH-TEMPERATURE
 WEAR BEHAVIOR OF FE-BASED AMORPHOUS COATINGS BY LASER CLADDING," *Materiali in tehnologije*, vol. 57, no. 4, Jul. 2023, doi: https://lo.17222/mit.2023.803.
- 385 [11] N. Magazov, Z. Satbaeva, B. Rakhadilov, and A. Amanov, "A Study on Surface Hardening and Wear 386 Resistance of AISI 52100 Steel by Ultrasonic Nanocrystal Surface Modification and Electrolytic Plasma 387 Surface Modification Technologies," *Materials*, vol. 16, no. 20, p. 6824, Oct. 2023, doi: 388 https://10.3390/ma16206824.
- C.-Y. Lee, T.-J. Lin, H.-H. Sheu, and H.-B. Lee, "A study on corrosion and corrosion-wear behavior of Febased amorphous alloy coating prepared by high velocity oxygen fuel method," *Journal of Materials Research and Technology*, vol. 15, pp. 4880–4895, Nov. 2021, doi: https://lo.1016/j.jmrt.2021.10.103.
- H. Han, M. Xiao, and Q. Wang, "Corrosion Performance of Fe-Based Amorphous Coatings via Laser Cladding Assisted with Ultrasonic in a Simulated Marine Environment," *Metals (Basel)*, vol. 13, no. 12, p. 1938, Nov. 2023, doi: https://10.3390/met13121938.

- J. Wu, Y. Wang, Q. Niu, and J. Zhang, "Study on fabrication technology and corrosion resistance of Fe-based amorphous alloy coatings by high-speed laser cladding," *J Phys Conf Ser*, vol. 2300, no. 1, p. 012009, Jun. 2022, doi: https://10.1088/1742-6596/2300/1/012009.
- 398 [15] M. Z. Ibrahim *et al.*, "Evolution of Iron-Based Metallic Glass Composite Coating with Enhanced Corrosion Resistance and Biocompatibility," *Arab J Sci Eng*, vol. 49, no. 8, pp. 10547–10559, Aug. 2024, doi: https://10.1007/s13369-023-08406-3.
- 401 [16] G. M. Uddin *et al.*, "Experimental study of tribological and mechanical properties of TiN coating on AISI 52100 bearing steel," *Advances in Mechanical Engineering*, vol. 10, no. 9, p. 168781401880288, Sep. 2018, doi: https://10.1177/1687814018802882.
- 404 [17] G. Lian, Y. Zheng, C. Chen, M. Feng, and X. Huang, "Influences of the composition design on the microstructure and properties of laser additive manufacturing TiAl alloy coatings," *Journal of Materials Research and Technology*, vol. 31, pp. 2543–2581, Jul. 2024, doi: https://10.1016/j.jmrt.2024.06.090.
- 407 [18] A. Maleque, S. Y. Cetin, H. H. Masjuki, and A. Hamdani, "Wear simulation of automotive engine component materials under biodiesel," *Journal of Mechanical Engineering and Sciences*, vol. 16, no. 4, pp. 9167–9174, Dec. 2022, doi: https://10.15282/jmes.16.4.2022.02.0726.
- 410 [19] M. A. Maleque, S. Y. Cetin, M. Hassan, M. Hafiz Sulaiman, and A. H. Rosli, "A systematic review on corrosive-wear of automotive components materials," 2022.
- 412 [20] J. Zhang, Y. Wang, Q. Niu, R. Fan, and J. Wu, "Study on toughening of Fe based amorphous coatings by ultra 413 high speed laser cladding," *J Phys Conf Ser*, vol. 2355, no. 1, p. 012075, Oct. 2022, doi: https://10.1088/1742-6596/2355/1/012075.
- 415 [21] H.-Z. Wang, Y.-H. Cheng, J.-Y. Yang, and Q.-Q. Wang, "Microstructure and properties of laser clad Fe-based amorphous alloy coatings containing Nb powder," *J Non Cryst Solids*, vol. 550, p. 120351, Dec. 2020, doi: https://10.1016/j.jnoncrysol.2020.120351.
- Z. Wang, J. Zhang, F. Zhang, and C. Qi, "Study on the microstructure and properties of a laser cladding Fe–Ni–Al coating based on the invar effect," *Sci Rep*, vol. 14, no. 1, p. 11685, May 2024, doi: https://10.1038/s41598-024-62306-6.
- J. Wu, Y. Wang, Q. Niu, and J. Zhang, "Study on fabrication technology and corrosion resistance of Fe-based amorphous alloy coatings by high-speed laser cladding," *J Phys Conf Ser*, vol. 2300, no. 1, p. 012009, Jun. 2022, doi: https://10.1088/1742-6596/2300/1/012009.
- 424 [24] H. Han, M. Xiao, and Q. Wang, "Corrosion Performance of Fe-Based Amorphous Coatings via Laser Cladding Assisted with Ultrasonic in a Simulated Marine Environment," *Metals (Basel)*, vol. 13, no. 12, p. 1938, Nov. 2023, doi: https://10.3390/met13121938.
- 427 [25] C. Chen, J. Wang, Y. Ge, M. Zhuang, and Z. Ma, "Microstructure and Wear Resistance of High-Chromium Cast Iron with Multicomponent Carbide Coating via Laser Cladding," *Coatings*, vol. 13, no. 8, p. 1474, Aug. 2023, doi: https://10.3390/coatings13081474.
- 430 [26] J. Zhang, Y. Wang, Q. Niu, R. Fan, and J. Wu, "Study on toughening of Fe based amorphous coatings by ultra 431 high speed laser cladding," *J Phys Conf Ser*, vol. 2355, no. 1, p. 012075, Oct. 2022, doi: https://10.1088/1742-6596/2355/1/012075.
- 433 [27] X. Ji, C. Luo, J. Juan, J. Zhao, and Y. Zhang, "Wear Resistance of Fe-Based Amorphous Powder Deposited Coatings in Air, Water, and SBF Solution: Effect of Layer Number," *Tribology Transactions*, vol. 65, no. 3, pp. 531–541, May 2022, doi: https://10.1080/10402004.2022.2054889.

- 436 [28] M. R. Najari, S. A. Sajjadi, and O. Ganji, "Microstructural evolution and wear properties of chromium carbide coating formed by thermo-reactive diffusion (TRD) process on a cold-work tool steel," *Results in Surfaces and Interfaces*, vol. 8, p. 100059, Aug. 2022, doi: https://lo.1016/j.rsurfi.2022.100059.
- 439 [29] X. Yao, J. Huang, Y. Qiao, M. Sun, B. Wang, and B. Xu, "Precipitation Behavior of Carbides and Its Effect on the Microstructure and Mechanical Properties of 15CrNi3MoV Steel," *Metals (Basel)*, vol. 12, no. 10, p. 1758, Oct. 2022, doi: https://10.3390/met12101758.
- H. Han, M. Xiao, and Q. Wang, "Corrosion Performance of Fe-Based Amorphous Coatings via Laser Cladding
 Assisted with Ultrasonic in a Simulated Marine Environment," *Metals (Basel)*, vol. 13, no. 12, p. 1938, Nov.
 2023, doi: https://10.3390/met13121938.
- 445 [31] H. Han, M. Xiao, and Q. Wang, "Corrosion Performance of Fe-Based Amorphous Coatings via Laser Cladding 446 Assisted with Ultrasonic in a Simulated Marine Environment," *Metals (Basel)*, vol. 13, no. 12, p. 1938, Nov. 447 2023, doi: https://10.3390/met13121938.
- 448 [32] Q. Li *et al.*, "Microstructure, wear and electrochemical behaviors of laser cladding Fe-based coatings with various molybdenum contents," *Mater Res Express*, vol. 9, no. 2, p. 026504, Feb. 2022, doi: https://10.1088/2053-1591/ac4e3d.
- J. Cheong, S. Wigger, H.-J. Füßer, and S. A. Kaiser, "High-resolution LIF-Imaging of the oil film thickness in the piston-ring / cylinder-liner contact in an optical tribometer," *Tribol Int*, vol. 147, p. 106230, Jul. 2020, doi: https://10.1016/j.triboint.2020.106230.
- 454 [34] X. Wang, Z. Lv, Y. Han, and J. Wang, "Effect of Grease Composition on Impact-Sliding Wear," *Lubricants*, vol. 12, no. 8, p. 279, Aug. 2024, doi: https://10.3390/lubricants12080279.
- 456 [35] C. Chen, J. Wang, Y. Ge, M. Zhuang, and Z. Ma, "Microstructure and Wear Resistance of High-Chromium Cast Iron with Multicomponent Carbide Coating via Laser Cladding," *Coatings*, vol. 13, no. 8, p. 1474, Aug. 2023, doi: https://10.3390/coatings13081474.
- 459 [36] D. Z. Segu and P. Hwang, "A comparative study of the friction and wear performance of Fe-based bulk metallic
 460 glass under different conditions," *Industrial Lubrication and Tribology*, vol. 69, no. 6, pp. 919–924, Nov.
 461 2017, doi: https://10.1108/ILT-12-2016-0308.
- 462 [37] Y. Wang *et al.*, "The investigation of tribological properties of PAI/PI-EPN polymer coating filled with WS2 and SiC at low temperatures," *J Appl Polym Sci*, vol. 141, no. 37, Oct. 2024, doi: https://10.1002/app.55953.
- H. Han, M. Xiao, and Q. Wang, "Corrosion Performance of Fe-Based Amorphous Coatings via Laser Cladding
 Assisted with Ultrasonic in a Simulated Marine Environment," *Metals (Basel)*, vol. 13, no. 12, p. 1938, Nov.
 2023, doi: https://10.3390/met13121938.
- 467 [39] L. Xie, Y. Wang, J. Yang, C. Li, X. Han, and J. Huang, "MICROSTRUCTURE AND HIGH-TEMPERATURE
 468 WEAR BEHAVIOR OF FE-BASED AMORPHOUS COATINGS BY LASER CLADDING," *Materiali in tehnologije*, vol. 57, no. 4, Jul. 2023, doi: https://lo.17222/mit.2023.803.
- 470 [40] C. Li, J. Zhai, L. Tian, Y. Lu, X. Li, and S. Kou, "Fabrication of Fe-based amorphous composite coating by laser cladding," *J Non Cryst Solids*, vol. 589, p. 121648, Aug. 2022, doi: https://10.1016/j.jinoncrysol.2022.121648.
- 473 [41] A. A. Sorour, A. Y. Adesina, M. A. Hussein, and B. F. Al-Daajani, "Effect of Powder Feed Rate of Plasma-474 Sprayed Fe–Cr–Mo–B–C Coatings on Microstructure, Tribology and Corrosion in 3.5% NaCl Solution," *Arab* 475 *J Sci Eng*, vol. 47, no. 7, pp. 9271–9285, Jul. 2022, doi: https://10.1007/s13369-022-06756-y.
- 476 [42] C. Chen, J. Wang, Y. Ge, M. Zhuang, and Z. Ma, "Microstructure and Wear Resistance of High-Chromium Cast Iron with Multicomponent Carbide Coating via Laser Cladding," *Coatings*, vol. 13, no. 8, p. 1474, Aug. 2023, doi: https://10.3390/coatings13081474.

- 479 [43] H. Han, M. Xiao, and Q. Wang, "Corrosion Performance of Fe-Based Amorphous Coatings via Laser Cladding 480 Assisted with Ultrasonic in a Simulated Marine Environment," *Metals (Basel)*, vol. 13, no. 12, p. 1938, Nov. 481 2023, doi: https://10.3390/met13121938.
- 482 [44] L. Xie, Y. Wang, J. Yang, C. Li, X. Han, and J. Huang, "MICROSTRUCTURE AND HIGH-TEMPERATURE
 483 WEAR BEHAVIOR OF FE-BASED AMORPHOUS COATINGS BY LASER CLADDING," *Materiali in tehnologije*, vol. 57, no. 4, Jul. 2023, doi: https://lo.17222/mit.2023.803.
- 485 [45] X. Mingying, X. Qiang, and J. Fengchun, "Effect of Copper Addition on the Phase Composition and Microstructure Evolution of Fe-Based Amorphous Alloy Coatings Prepared by Laser Cladding," *Advances in Materials Science and Engineering*, vol. 2022, pp. 1–7, Apr. 2022, doi: https://10.1155/2022/3511432.
- 488 [46] C. Li, J. Zhai, L. Tian, Y. Lu, X. Li, and S. Kou, "Fabrication of Fe-based amorphous composite coating by laser cladding," *J Non Cryst Solids*, vol. 589, p. 121648, Aug. 2022, doi: https://10.1016/j.jnoncrysol.2022.121648.
- 491 [47] H. Zhang, Y. Liu, X. Bai, W. Zhao, P. Zhang, and W.-F. Rao, "Laser cladding highly corrosion-resistant nano/submicron ultrafine-grained Fe-based composite layers," *Surf Coat Technol*, vol. 424, p. 127636, Oct. 2021, doi: https://10.1016/j.surfcoat.2021.127636.
- L. Chen, T. Yu, C. Guan, and Y. Zhao, "Microstructure and properties of metal parts remanufactured by laser cladding TiC and TiB2 reinforced Fe-based coatings," *Ceram Int*, vol. 48, no. 10, pp. 14127–14140, May 2022, doi: https://10.1016/j.ceramint.2022.01.299.
- 497 [49] L. Xie, Y. Wang, J. Yang, C. Li, X. Han, and J. Huang, "MICROSTRUCTURE AND HIGH-TEMPERATURE
 498 WEAR BEHAVIOR OF FE-BASED AMORPHOUS COATINGS BY LASER CLADDING," *Materiali in tehnologije*, vol. 57, no. 4, Jul. 2023, doi: https://lo.17222/mit.2023.803.
- 500 [50] X. Hou, D. Du, B. Chang, and N. Ma, "Influence of scanning speed on microstructure and properties of laser cladded Fe-based amorphous coatings," *Materials*, vol. 12, no. 8, 2019, doi: https://10.3390/ma12081279.
- 502 [51] J. Zhang, Y. Wang, Q. Niu, R. Fan, and J. Wu, "Study on toughening of Fe based amorphous coatings by ultra 503 high speed laser cladding," *J Phys Conf Ser*, vol. 2355, no. 1, p. 012075, Oct. 2022, doi: https://10.1088/1742-6596/2355/1/012075.
- 505 [52] L. Xie, Y. Wang, J. Yang, C. Li, X. Han, and J. Huang, "MICROSTRUCTURE AND HIGH-TEMPERATURE
 506 WEAR BEHAVIOR OF FE-BASED AMORPHOUS COATINGS BY LASER CLADDING," Materiali in tehnologije, vol. 57, no. 4, Jul. 2023, doi: https://lo.17222/mit.2023.803.
- 508 [53] G. Kim *et al.*, "Microstructural Evolution, Hardness and Wear Resistance of WC-Co-Ni Composite Coatings Fabricated by Laser Cladding," *Materials*, vol. 17, no. 9, p. 2116, Apr. 2024, doi: https://10.3390/ma17092116.
- 510 [54] H. Han, M. Xiao, and Q. Wang, "Corrosion Performance of Fe-Based Amorphous Coatings via Laser Cladding
 511 Assisted with Ultrasonic in a Simulated Marine Environment," *Metals (Basel)*, vol. 13, no. 12, p. 1938, Nov.
 512 2023, doi: https://10.3390/met13121938.
- 513 [55] A. A. Sorour, A. Y. Adesina, M. A. Hussein, and B. F. Al-Daajani, "Effect of Powder Feed Rate of Plasma 514 Sprayed Fe-Cr-Mo-B-C Coatings on Microstructure, Tribology and Corrosion in 3.5% NaCl Solution," *Arab* 515 *J Sci Eng*, vol. 47, no. 7, pp. 9271–9285, Jul. 2022, doi: https://10.1007/s13369-022-06756-y.
- 516 [56] A. A. Sorour, A. Y. Adesina, M. A. Hussein, and B. F. Al-Daajani, "Effect of Powder Feed Rate of Plasma-517 Sprayed Fe-Cr-Mo-B-C Coatings on Microstructure, Tribology and Corrosion in 3.5% NaCl Solution," *Arab* 518 *J Sci Eng*, vol. 47, no. 7, pp. 9271–9285, Jul. 2022, doi: https://10.1007/s13369-022-06756-y.
- 519 [57] H. Han, M. Xiao, and Q. Wang, "Corrosion Performance of Fe-Based Amorphous Coatings via Laser Cladding 520 Assisted with Ultrasonic in a Simulated Marine Environment," *Metals (Basel)*, vol. 13, no. 12, p. 1938, Nov. 521 2023, doi: https://10.3390/met13121938.